Revised version, modifications highlighted in color YELLOW

# Fatigue Assessment of Steel Riveted Railway Bridges: Full-Scale Tests and Analytical Approach.

Elisa Bertolesi [a]*, Manuel Buitrago [b], Jose M. Adam [b, c], Pedro A. Calderón [b, c]

[a] Department of Civil and Environmental Engineering, Brunel University London, UB8 3PH Uxbridge, UK

[b] ICITECH, Universitat Politècnica de València, Camino de Vera s/n, 46022 Valencia, Spain

[c] CALSENS, Camino de Vera s/n, 46022 Valencia, Spain

* Corresponding author: elisa.bertolesi@brunel.ac.uk

**Keywords:** Fatigue, Structural Health Monitoring, Steel bridges, Truss structures, Full-scale tests.

## Abstract

This paper describes a double experimental and analytical study of the fatigue behaviour of the Quisi and Ferrandet Bridges, twin 170 m long steel railway bridges constructed between 1913 and 1915 with typical Pratt truss structures and riveted connections. These bridges are part of the Spanish national railway network connecting the towns of Alicante and Denia, one of the key networks in the Valencia Region (Spain). The experimental laboratory investigation involved fatigue testing in one of the ICITECH laboratories at the *Universitat Politècnica de València* of: (i) a full-scale bridge span and (ii) an upper cross beam from the Ferrandet bridge. During the tests, Linear Variable Displacement Transducers (LVDTs) and Strain Gauge (SG) sensors were used to capture the possible nucleation and propagation of fatigue cracks. Fatigue test carried out on the cross beam identified: (i) fatigue life of the critical detail, (ii) fatigue hot-spots along the cross beam and (iii) strain redistribution along the riveted element during crack growth. The experimental results from the full-scale bridge were adopted to calibrate an elastic numerical model of the whole structure, which was in turn used to estimate the Quisi Bridge's remaining fatigue life. The definition of the class of detail and remaining fatigue life were calculated by the S-N curves method, according to Eurocode 3, considering the available information on the bridges' loading histories.

Revised version, modifications highlighted in color YELLOW

# 1. Introduction

Most steel bridges designed between the early 19th century and the mid-20th century were built of structural steel with riveted joints. The fatigue behaviour of riveted joints has become a topic of interest due to the large number of bridges of this type still in service despite the heavy traffic volumes they have sustained over the years. A fact that deserves special mention is that more than 60% of the railway bridges in Europe are over 50 years old and more than 30% are over 100 years old [1]-[9]. Most of these bridges were built prior to standardization [10][11][12][13] and the widespread use of design codes, and now are subjected to higher loads and speeds than those for which they were originally designed. Many therefore require maintenance and in some cases need to be partially or completely replaced.

Due to the large number of riveted steel railway bridges in Europe, replacing all these structures will be extremely costly and virtually impossible unless phased over several decades [7]. The riveted connection construction technique has been one of the most durable techniques in the history of steel bridges and was the preferred system until the 20th century [5][6]. In spite of this, the damage statistics of various steel structures clearly demonstrate that steel bridges are 38% more likely to fail due to fatigue crack propagation [1]. Several studies [2][4][8] indicate that old riveted bridges suffer from a combination of multiple aspects, including construction material characteristics and degradation, while [2] points out that old riveted bridges were mainly constructed using puddle iron and mid-low carbon steel. The combination of heterogeneous material and slag with low C and Si contents favour degradation processes and reduce the steel's chemical and mechanical resistance to microstructural damage and promote the nucleation of fatigue cracks. These findings also apply to other types of steel bridges constructed in the same era.

Microstructural damage is likely to affect the structural behaviour of steel bridges only at an advanced state of crack propagation. The observations of studies adopting multiple approaches highlighted their high structural redundancy as a common feature. This means that the failure of a component generally does not lead to the gradual collapse of the entire structure, since a crack in a riveted girder will most likely remain within the cracked component. In this situation the rivets help the compartmentation of the damage in the cracked girder and prevent it from spreading to other elements. However, after the failure of one element and the distribution of the loads to the remaining components, a progressive failure can start or there may even be a new fatigue failure due to the higher cyclic loads they receive. In-field monitoring of steel railways bridges [14]-[17] is therefore of paramount importance in understanding the actual state of steel structures subjected to cyclic loads.

The authors of [16] pointed out that fatigue damage is expected to occur in primary elements, mostly in stringers and cross beams, which directly bear the cyclic loads. Similar findings emerged in [18]-[20], when the authors analysed the fatigue behaviour of riveted connections. Advanced numerical studies later confirmed by experimental tests [21] revealed that the angle fillet and the rivet head-to-shank junction and holes are fatigue-starting hot-spots. The authors of [18] demonstrated by means of several parametric FE analyses that defects can affect the fatigue behaviour of riveted connections in the presence of: (i) clearance between the rivet shank and rivet hole and (ii) the loss of a rivet. The authors in [22] analysed the behaviour of stringer-to-floor beam connections in old riveted bridges and underlined that primary elements are the most prone to experience fatigue failures because they are usually short in length and accumulate large stress fluctuations. The fatigue tests performed by the authors also revealed that riveted connections performed better than expected, assuming detail class 71, thus, confirming that it is a safer assumption in the absence of experimental data [22]. They also found that the state of stress is strongly influenced by the connection quality and thus its end-fixity plays a crucial role.

Considering the level of skill required to produce riveted connections and the absence of standardized quality controls, it is not surprising that the authors detected high uncertainty related to the determination of rivet fatigue strength. Among the experimental works carried out on riveted elements, it is worth mentioning the investigations carried out in [23][24]. In [23] the authors performed a wide experimental and analytical investigation on riveted railway bridge girders and subjected them to full-scale bending tests. The lab tests confirmed that the critical point in the bridge was the riveted connections of the shear-diaphragms directly carrying the loads. Fatigue failure also originated in rivet shanks and resulted in their head loss. Finally, a detail category of 117 was suggested. In [24] the authors experimentally analysed the behaviour of a 12.4 m long railway bridge. In agreement with [22] and [23], Pipinato et al. identified the riveted connections of the shear diaphragms carrying the rails as the bridge's fatigue hot-spot, mainly in the rivet shanks. The analytical studies confirmed that a detail class of 100 should be preferred in case of failure triggered by tangential stresses (shear stresses). This finding is partially in agreement with Eurocode 3 recommendations that suggest detail classes 80 and 100 should be adopted.

From a structural point of view, few studies [25][26] in the literature deal with the experimental fatigue testing of full-scale riveted bridges or subassemblies due to the huge financial and operational implications. The aim of the present study was to enrich the broader scenario of experimental fatigue studies of riveted elements with a double experimental and analytical study dealing with: (i) a full-scale span of a riveted steel railway bridge after more than 100 years of operational service and (ii) a full-scale localized fatigue test of a cross beam. The results obtained from the two lab tests were coupled with load tests on bridges, Linear-Static Finite-Element Analysis (LSFEAs) and the current recommendations to define an integrated multi-field analytical method for predicting the residual fatigue life of steel bridges. The proposed approach could be extended to other bridges on the basis of: (i) real loading tests and (ii) numerical simulations, assuming detail categories 71 and 100, according to whether the expected failure mechanism is normal or tangential. This method was also applied in this work to the Quisi Bridge, which is still in service.

The paper is organized as follows: After this Introduction, Section 2 describes the bridge geometry, while Section 3 describes the method used in the study. Sections 4 and 5 report the results obtained from both studies and Section 6 discusses the analytical approach adopted to estimate the detail class and the bridge's residual fatigue life. Section 7 summarizes the most important findings obtained and outlines future work.

## 2. Geometrical description of the Quisi and Ferrandet Bridges

These Pratt truss bridges are part of the Spanish national railway network connecting the towns of Alicante and Denia and were constructed between 1913 and 1915. As can be seen in **Figure 1**, the Quisi Bridge is approximately 170 m long and is composed of 6 spans with lengths varying between 21 and 42 m resting on two lateral abutments (LA 1 and 2) and five steel truss columns (P1, P2, P3, P4 and P5) of different heights fixed to ashlar foundations. The two central spans form a continuous hyperstatic beam (spans 3 & 4), while the lateral spans 1, 2, 5 and 6 were constructed as isostatic elements. The span nomenclature and main geometrical details are also reported in **Figure 1** and **Figure 2**.

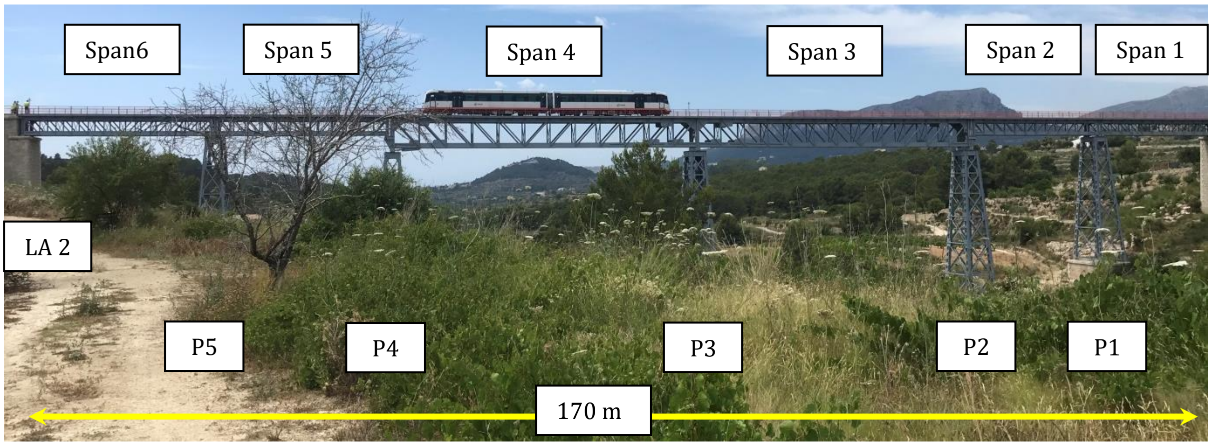


**Figure 1:** Quisi bridge geometry and span nomenclature.

After more than 100 years in service and due to the general increase in rail traffic, the railway company activated different restoration strategies for steel bridges, one of which involved replacing the Ferrandet Bridge by a completely new structure. This gave us a unique opportunity to move one of its spans, with the same geometry as spans 2 and 5 of the Quisi Bridge, to the ICITECH laboratories at the *Universitat Politècnica de València* (Valencia, Spain), where it was tested under fatigue loads. The results obtained can be extended to other similar railway bridges (like the Quisi Bridge, **Figure 2**), with the same geometry.

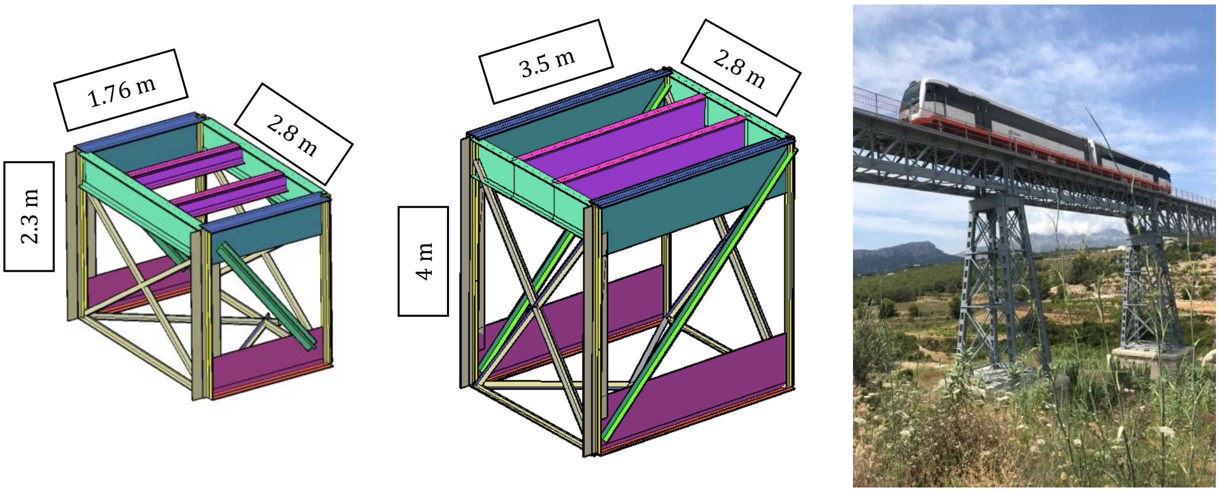


-a -b -c

**Figure 2:** Quisi bridge: geometry of the isostatic (-a) and iperstatic (-b) modules and (-c) 3D view of piers 4 and 5.

# 3. Experimental investigation

## 3.1 Methodology

The study was organized into two parts: a laboratory study and an analytical assessment. The experimental results were used to validate the current recommendations proposed by Eurocode 3 and extend our knowledge of fatigue failures in old riveted steel elements. It was considered of paramount importance to test riveted bridge structures after years of operational service and environmental degradation. Since fatigue tests on full-scale bridges under controlled laboratory conditions have obvious technical limitations, it was decided to carry out a double experimental investigation on two different scales. One of the lab tests was on an upper cross beam subjected to railway load cycles and thus vulnerable to fatigue damage. The second, and more ambitious, lab test was applying cyclic loads to a full-scale isostatic bridge span.

The first test identified the following data: (i) maximum number of cycles before fatigue failure, (ii) identification of fatigue hot-spots inside the element, (iii) the precision, position and utility of the different SG and LVDT sensors and (iv) crack growth rates. The information from (i) allowed us to define the detail class by adopting the S-N curves method proposed in [10][11][13][26] (see below). The data provided by (ii), (iii) and (iv) identified effective fatigue-crack monitoring strategies. The results from the second investigation were used to calibrate a Finite Element numerical model for the analytical assessment. The overall findings were: (i) the identification of the elements most vulnerable to fatigue failure, and (ii) the expected operational life up to fatigue failure.

### 3.2 Preliminary assessment of materials

The following tests were performed on different samples from the bridges: (i) tensile tests according to EN ISO 6892-1 [27] (ii) the Charpy impact test according to EN ISO 148-1 [28] and (iii) mineralogical and chemical tests. The mechanical and impact test results are summarized in **Table 1** and **Table 2**. All the tested samples showed consistent results in terms of both yielding and ultimate strengths, while the impact results were widely scattered. The good quality of the steel comparable with that of current steel can be seen in the results in Table 1.

**Table 1:** Quisi and Ferrandet bridges: tensile test results.

| Sample | Yielding strength [MPa] | Ultimate strength [MPa] | Elongation [%] |
|---|---|---|---|
| **Quisi** | 271 | 399 | 32 |
| **Ferrandet** | 299 | 325 | 36 |

**Table 2:** Quisi and Ferrandet bridges: Charpy impact test results (Joule).

| Sample | Temperature [°C] | |
|---|---|---|
| | 0 | 20 |
| **Quisi** | 32 | 64 |
| **Ferrandet** | 18 | 34 |

The chemical results are summarized in **Table 3** for different types of samples (rivet, plate and profile). According to [2], the brittle nature of old riveted bridges is associated with the presence of impurities and low C and Si content steel (<0.1% and 0.03%, respectively). The Ferrandet Bridge clearly shows these features while the Quisi Bridge has higher C and Si contents.

**Table 3:** Chemical test results of Quisi and Ferrandet Bridges (%).

| Bridge | Sample | C | Si | Mn | P | S | Cr | Ni | Mo |
|---|---|---|---|---|---|---|---|---|---|
| Quisi | Rivet | 0.193 | 0.018 | 0.492 | 0.060 | >0.130 | - | - | - |
| Ferrandet | | 0.037 | 0.036 | 0.33 | 0.048 | 0.063 | - | - | - |
| Quisi | Plate | 0.139 | 0.108 | 0.520 | 0.079 | 0.072 | - | - | - |
| Ferrandet | | 0.046 | <0.017 | 0.336 | 0.063 | 0.089 | - | - | - |
| Quisi | Profile | 0.139 | 0.105 | 0.510 | 0.066 | 0.071 | - | - | - |
| Ferrandet | | 0.042 | <0.017 | 0.346 | 0.041 | 0.050 | - | - | - |

# 4. Riveted cross beam element

## 4.1 Fatigue load protocols and experimental set-up

The geometry of the tested element is shown in **Figure 3-a**, while **Figure 3-b** depicts the experimental set-up adopted.

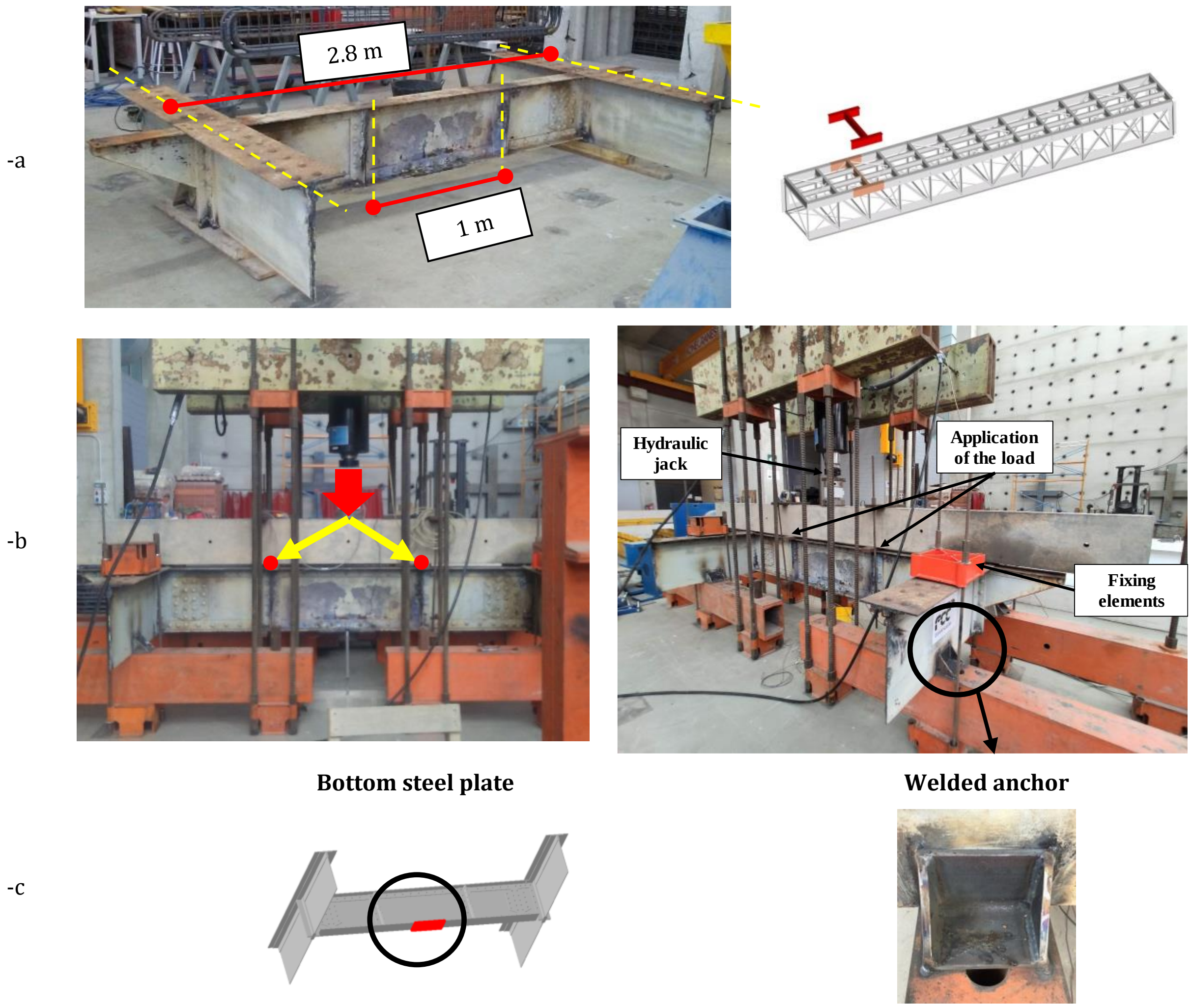


**Figure 3:** Geometry of the riveted truss beam tested (-a), experimental set-up (-b) and details of the beam and welded anchors (-c).

The experimental set-up comprised the application of a 0.55 Hz frequency cyclic load (maximum speed of the hydraulic jack) ranging from 50 to 650 kN, redistributed at two points by a stiff beam designed to simulate load transfers in real traffic scenarios. The loading points were in fact under the railway tracks. The load range and frequency were determined in order to exploit the maximum capability of the hydraulic jack used during the investigation. To this scope, the experimental design stress range was designed to reasonably minimize the number of cycles (using S-N curve method) whilst preventing the structures to experience any plastic deformation that could trigger (or anticipate) the formation of fatigue cracks. The same strategy was used when designing the experimental test on the full-scale span bridge. Lateral restraints play a crucial role in the stress state of the riveted beam when subjected to cyclic loads, when the riveted beam is mainly subjected to bending transmitted to the lateral chords by the riveted connections. The riveted beam was firmly anchored to the reaction floor by four lateral welded anchors positioned so that they did not introduce additional stiffness to the lateral restraints. A detail of the anchorage can be seen in **Figure 3-b-c**.

**Table 4:** Description of sensor positions

| Sensor | Position | Sensor | Position |
|---|---|---|---|
| SG 1 | Centre, lateral bottom part of the web | LVDT 1 | Mid-span |
| SG 2 | Centre, mid lower flange | LVDT 2 | Lateral riveted connection |
| SG 3 | Centre, mid lateral lower flange | | |
| SG 4 | Centre, mid upper flange | | |

The fatigue behaviour of the riveted element was monitored by four strain gauges (SG) and two Linear Variable Displacement Transducers (LVDT). **Figure 4** shows the sensor network, while **Table 4** gives their positions. Fatigue cracks can be initiated by abrupt local changes in the cross section, such as by the presence of an additional steel plate anchored to the beam bottom flanges (see **Figure 3**). One LVDT was positioned below the tested element to monitor vertical deflections and another to evaluate possible relative movements between rivet head and the lateral profile indicating a possible weak point of the cross beam.

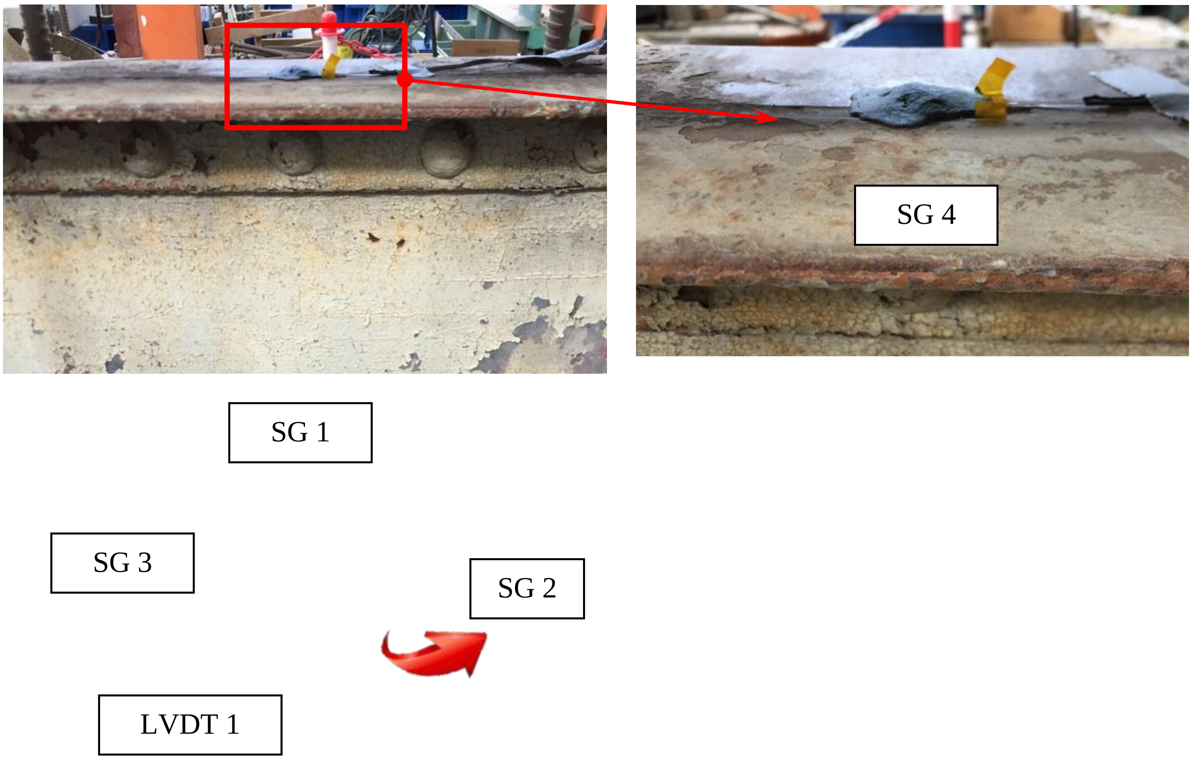


**Figure 4:** Position of the sensors: strain gauges and Linear variable Displacement Transducers.

## 4.2 Experimental Results

The riveted cross beam element can be seen in **Figure 3-a**. **Figure 5** gives the experimental envelopes obtained monitoring strain gauges SG1, SG2, SG3, SG4, and LVDT 1 and LVDT 2**.** Similarly, **Figure 6** gives the strain increment history obtained by the four strain gauges at the beam mid-span subjected to a constant cyclic load range of 600kN. The strain increment (**Figure 7**) was calculated as the absolute difference between maximum and minimum strains recorded in each cycle. All the sensors monitored similar strain increment trends in four different stages (see **Figure 6**). In the first, there was an initial transitory period of approximately 100 cycles to stabilize the beam's cyclic response, after which the behaviour was stable until approximately the $10000^{th}$ cycle (stage 2), when a fatigue crack started. At 12k cycles, the strain increment trends abruptly changed due to the rapid propagation of a fatigue crack (stages 3 and 4), which involved a gradual loss of cross beam flexural stiffness and stress redistribution. The strain increments either increased or decreased according to the position of the sensor and the quality of the riveted connection (**Figure 6**).

The cross beam failed at approximately 31k cycles. Between cycles 0.1k and 10k, when the behaviour of the cross beam was almost elastic, the strain distribution along the mid-section was not as expected by classic beam theory. According to the literature [2][23][24], the quality of the connections together with high uncertainty plays a crucial role in redistributing the strains in the beam elements. Despite this, the sensors were able to deal with the different stress redistribution as the cracks grew. SG 2 and 3 detected a fatigue crack at an early stage. These sensors monitored varying rates of strain reduction, while, SG1 detected the expected rise of the strain increments (see **Figure 5-a**). This behaviour was caused by the strain redistribution along the element. SG4, on the upper compressed surface, showed a smoother increase of the strain increments than the others (see **Figure 5 -d**). As expected, the SG sensors were all able to warn of the changes in the cross beam's behaviour. Those close to the cracks (i.e. SG 1, 2 and 3) clearly detected the formation and propagation of cracks at an early stage, while SG 4 was the worst at replicating the spread of the structural failure (see **Figure 5 -a-b-c and -d**).

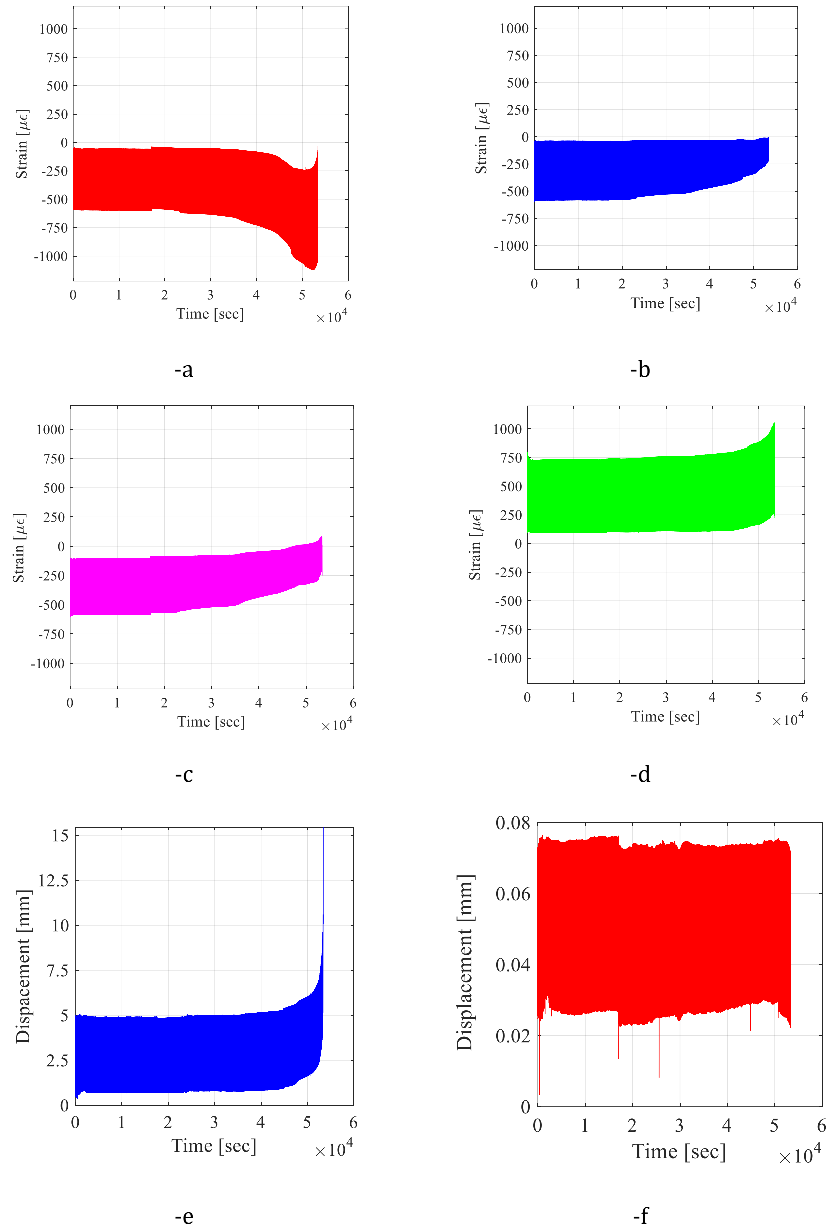


**Figure 5:** Fatigue test result envelopes: strain gauge SG 1 (-a), SG 2 (-b), SG 3 (-c), SG 4 (-d) (negative strains mean traction) and LVDT1 (-e), LVDT2 (-b).

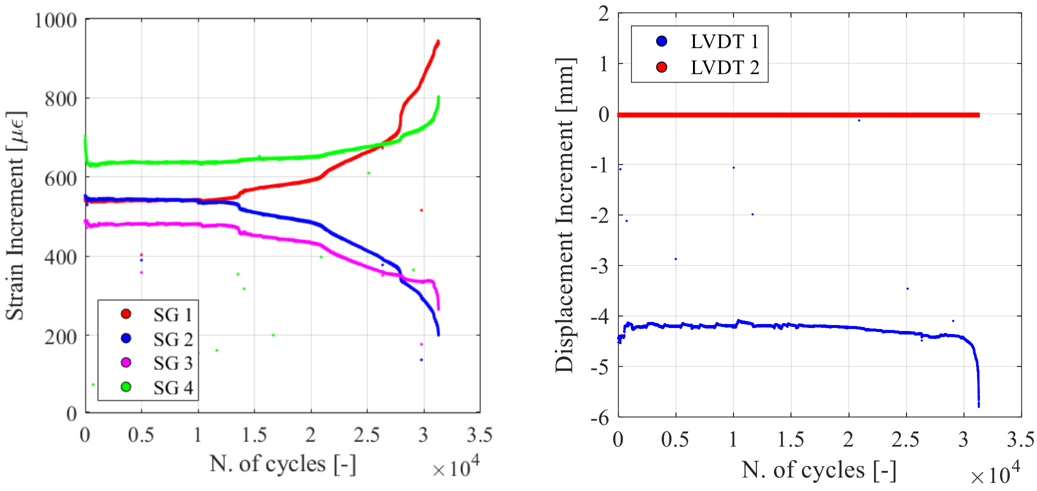


-a -b

**Figure 6:** Strain (-a) and displacement (-b) increment histories.

A quite different trend was observed in the two LVDTs on the cross beam. LVDT 1 recorded the vertical displacements in the mid-section and LVDT 2 the possible relative movements at one of the lateral riveted connections. As can be seen in **Figure 5-e and -f and Figure 6-b**, there were no relative displacements at the lateral joint, showing that the riveted connection maintained its integrity. Conversely, LVDT 1 recorded a fairly smooth increase of the mid-span vertical displacements until approximately 30k cycles, when the cross beam element was about to fail. Deformation sensors (such as SG) are preferable to displacement sensors because they provide much more information about the local formation and propagation of fatigue cracks, especially in elements subjected to bending such as primary girders.

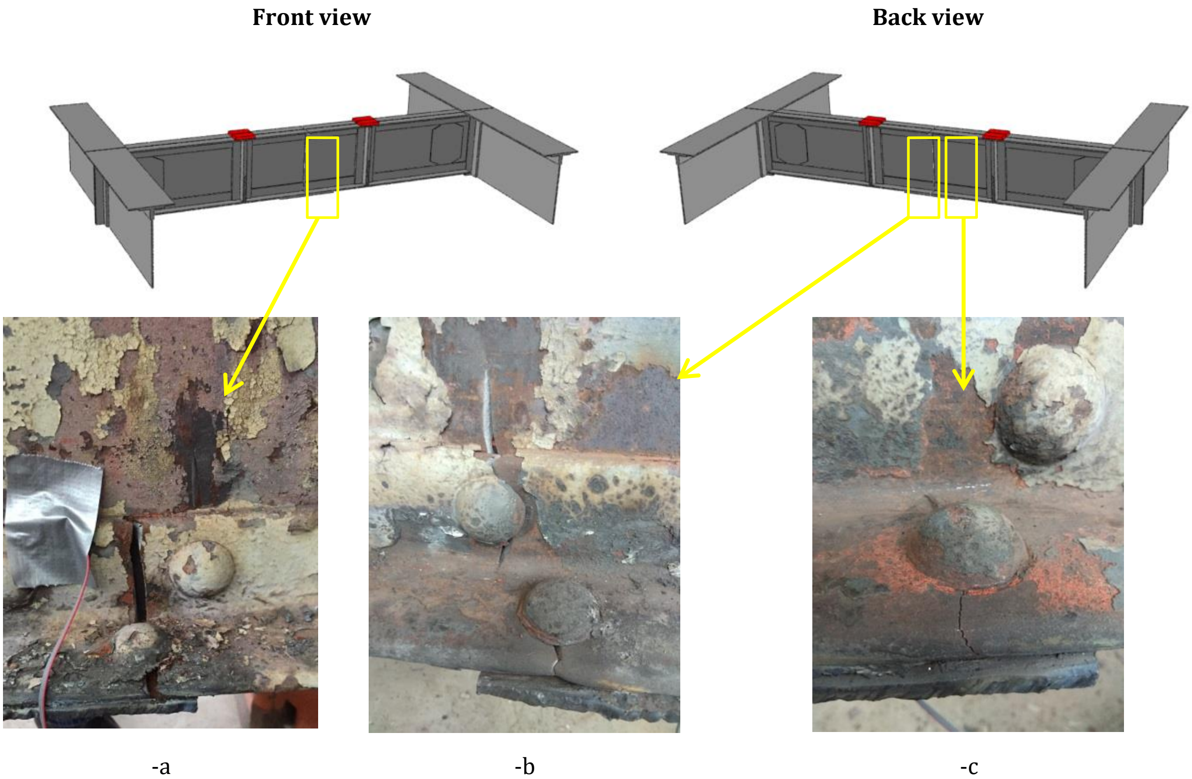


**Figure 7:** Fatigue cracks observed at the end of the experimental investigation: front (-a) and back (-b) views of first fatigue crack and (-c) back view of the second crack.

**Figure 7** shows the crack patterns at the end of the lab test. The cross-beam element has three similar fatigue cracks at the edges of the cross beam mid-span plate. The mid-span section comprised one steel plate anchored to the bottom flange which was anchored to the vertical web. It should be noted that all the joints were riveted. This particular construction technique is prone to the following issues: (i) a local change of the cross beam flexural stiffness at the ends of the bottom plate and (ii) a reduction of the bottom flange section due to the presence of rivets. According to the literature, the most severe cracks begin in the last rivet connecting the bottom flange to the steel plate, as can be seen in **Figure 7**. The crack then propagated until compromising the bottom flange and reached the vertical web. In this case, the different elements composing the girder and connected by rivets were not able to stop the crack propagation. Indeed, one fatigue crack severely damaged the vertical web in a symmetrical pattern, which was probably due to the flexural behaviour of the cross beam. During the lab test, the fatigue crack front propagated from the bottom flanges to the vertical web due to the higher stresses caused by the progressive drop in the beam's flexural stiffness caused by the damage itself. It is also interesting to note that another two cracks opened on the opposite plate edge (see **Figure 7**) but were narrower than the first and did not reach the web.

# 5. Full-scale riveted steel bridge

## 5.1 Fatigue load protocols and experimental set-up

A 21 m long isostatic span from the Ferrandet Bridge was moved to the ICITECH laboratories at the *Universitat Politècnica de València* (Spain) (see **Figure 8**). In the laboratory, the bridge was positioned on two hinged and two simple supports (see **Figure 9**). A cyclic load was then applied ranging from 50 to 1300 kN at a frequency of 0.2 Hz (maximum load and speed of the hydraulic jack) by means of a hydraulic jack positioned vertically over the centre of the span, redistributing the load at four points by means of three stiff beams (green and yellow in **Figure 9**).


-a -b -c

**Figure 8:** Movement phases: taking from storage area (-a), movement (-b) and laboratory placement (-c).

The bridge's structural response was monitored by 40 strain gauges (SG) and 8 Linear Variable Displacement Transducers (LVDTs) collecting data at a sampling rate of 50Hz.

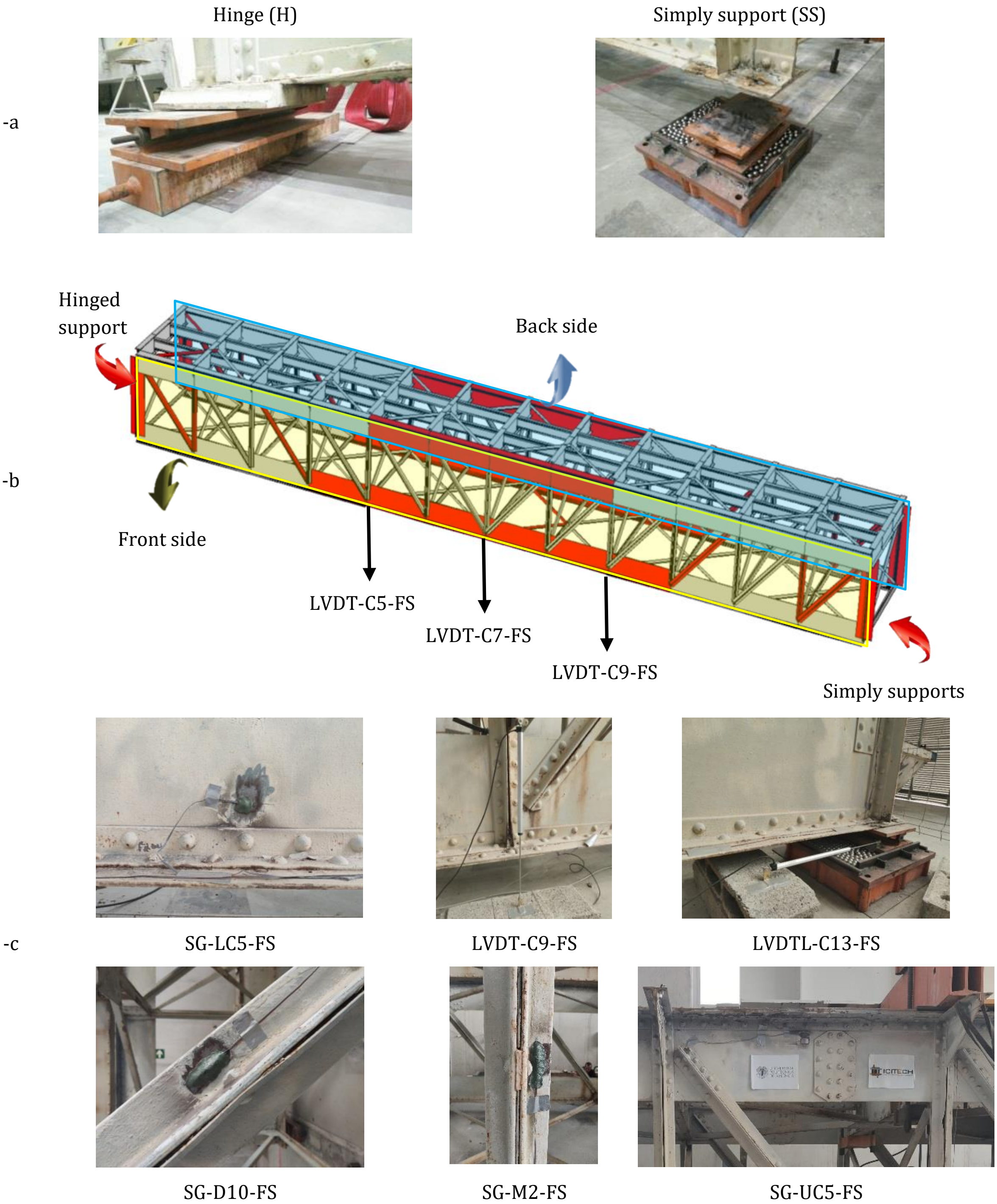


**Figure 9:** Experimental set-up and sensor network: types of supports (-a), nomenclature details (-b) and types of sensors (-c).

The sensor positions are shown in **Figure 9**: (i) position and orientation of the LVDTs (blue lines) and (ii) structural elements with SGs (red lines), which comprised: upper and lower central chords, lateral diagonals, vertical truss and upper and lower horizontal bracings. The SG sensors were placed at the centre of mass of the elements (such as upper and lower chords) and at the centre of each element length. The LVDTs were placed: (i) on the central vertical columns to monitor the maximum vertical displacements, and (ii) close to the lateral supports to study the transversal and longitudinal movements of the whole structure. The sensor nomenclature followed the general rule: X-YN-Z, where X indicates the sensor type (i.e. SG for strain gauges and LVDT for Linear Variable Displacement Transducers), Y means the element to which the sensor is applied (i.e. C=vertical columns, UP=upper chord, LC=lower chord, D=diagonal, CRV=vertical crux, CRHU=upper horizontal crux and CRHL= lower horizontal crux), N indicates the number of the element starting from the hinged side and Z stands for the position of the element (i.e. FS=front, BS=rear). The horizontal LVDT nomenclature also indicates the sensor orientation (i.e. L and T stand for longitudinal and transversal, respectively).

## 5.2 Experimental Results

The strain gauge results are depicted in **Figure 10** and include: vertical struts, diagonal elements, upper and lower chords and horizontal bracing. For the sake of brevity, since the fatigue test was over 45k cycles (equivalent to an extra of 27 years more of operational service), only the first and last cycle stress ranges are compared. The calculation of the equivalent number of years was performed considering the strain increment monitored during the laboratory test on the most loaded bottom chord and transforming this value in a stress range (92 MPa) using the elastic modulus of steel. With this stress range, together with the consideration or the real detail category of the structure (see Section 6.3 for more details) and applying the S-N curves methodology, the structure is able to withstand approximately 624k cycles until reaching the collapse of the structure. Since during the lab test 45k cycles were applied to the riveted span, the damage accumulated during the laboratory campaign was equal to approximately 7.2%. Therefore, considering an appropriate behaviour of the structure under fatigue loading until a level of damage of 7.2%, and also taking into account a series of data for the future traffic volume and characteristics (e.g. the maximum real stress of the most loaded bottom chord of the structure is 42.1MPa which is a value monitored in a real field test of the structure, the train passes over the bridge for the future corresponds to the Type 9, 32 circulations per day; see Section 6.4 for more details) and the S-N curves methodology, a number of cycles equal to 320k may be withstood by the structure, which could be attained in 27 years. The stress ranges were deduced from the strain increments from the sensors and multiplied by the steel Elastic Modulus (210 GPa). In **Figure 10-a** it can be seen that there is a low scatter between the increments in elements C1-FS and C1-BS and on their opposite counterparts C13-FS and C13-BS. Similar findings could be deduced from the results in **Figure 10-b, -c and –d**, showing almost symmetrical bridge behaviour in both directions. As expected, the stress distribution along the structural elements comprised the central lower chords subjected to higher stress ranges (LC6-FS/BS and LC7-FS/BS). Similarly, higher compressive stresses were obtained in the upper counterparts (UP6-FS/BS and UP7-FS/BS). Diagonals D3-

FS/BS and D10-FS/BS were the two subjected to the highest stresses. The shear loads were higher on the external diagonals and vertical columns, although the stresses were higher in other elements due to having smaller cross-sections. Three general observations can be made: (i) the stress level in all the elements is far lower than the elastic limit obtained from the lab tests reported in Section 3, (ii) none of the elements analysed in the present study obtained more than a 5% difference between the first and the last cycles; and (iii) visual inspection did not reveal any damage in the structure.

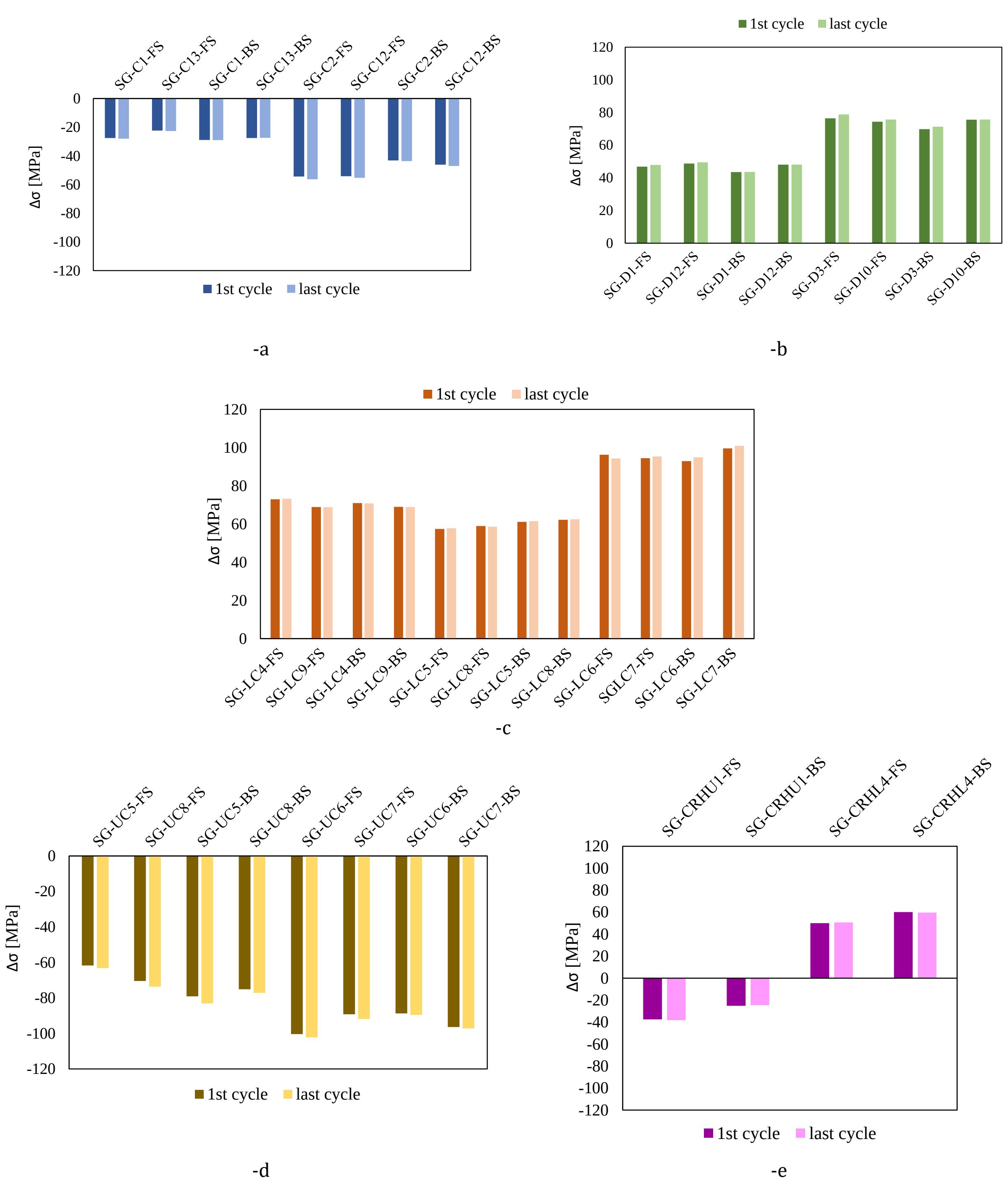


**Figure 10:** Stress range computed at the beginning and at the end of the test in: (-a) columns, (-b) diagonals, (-c)

upper chords, (-d) lower chords and (-e) bracing cruxes.

**Figure 11** gives the displacement increments read by the LVDTs on the central portion of the bridge (LVDT-C5-FS/BS, LVDT-C7-FS/BS and LVDT-C9-FS/BS) and those that monitored the longitudinal and transversal movements of the structure (LVDTL-C13-FS and LVDTT-C13-FS/BS). As expected, the maximum vertical displacements were observed in the centre of the bridge. As in **Figure 10**, displacement increments did not vary between the first and last cycle, again confirming the absence of damage and the elastic behaviour of the bridge. LVDTT-C13-FS monitored the possible presence of transversal displacement of the support. As shown in **Figure 11**, there were negligible movements in that direction.

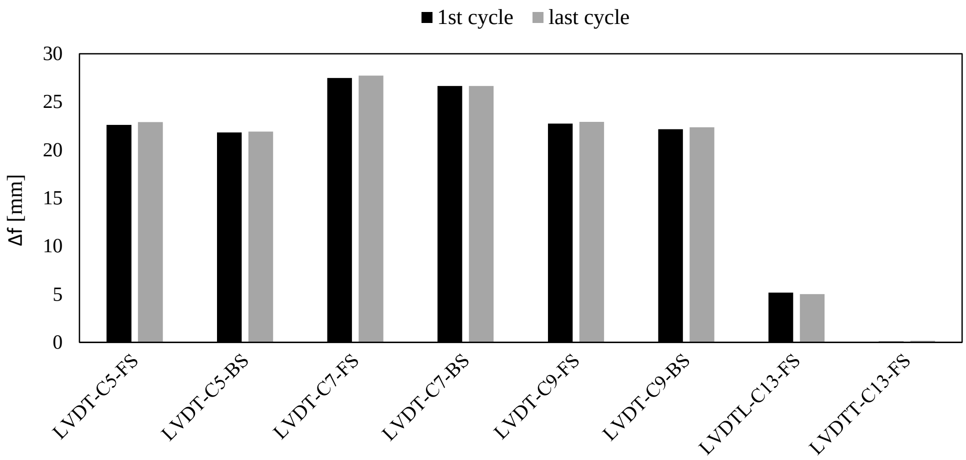


**Figure 11:** Displacement increment computed at the beginning and at the end of the fatigue test.

The experimental results were also compared to the numerical outputs obtained using a 3D Linear-Static Finite-Element model (LSFE). The isostatic span tested during the lab investigation was modelled by means of two-noded beam elements, as shown in **Figure 12-a**.

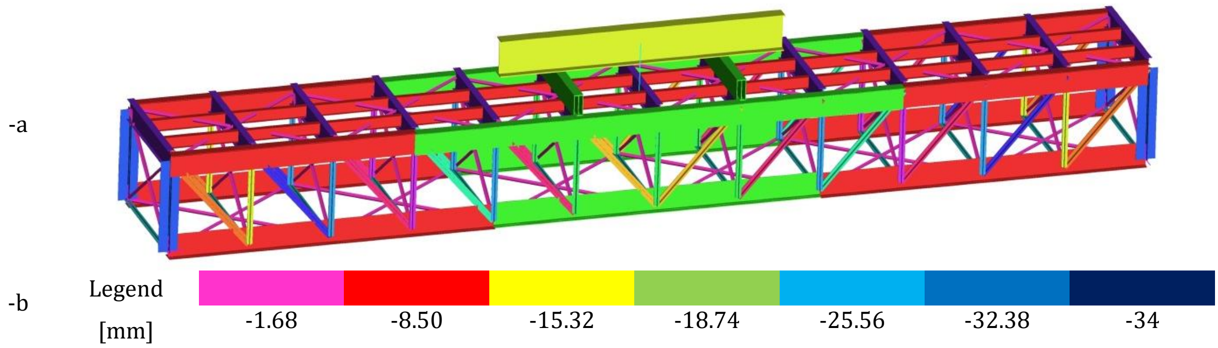

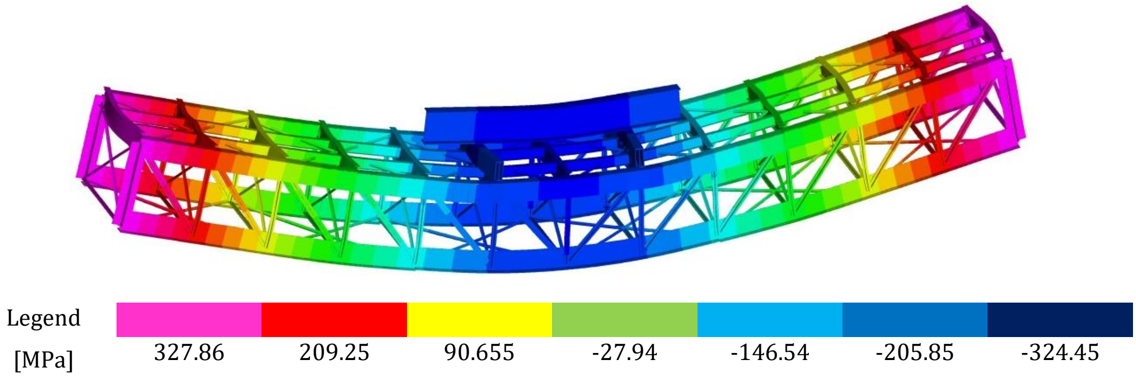


-c

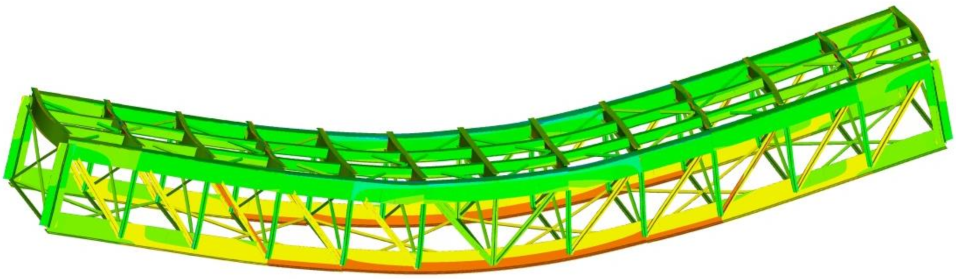

**Figure 12:** Finite Element model developed to analyse the behaviour of the isostatic span tested during the lab investigation (-a), vertical displacements (negative downwards) (-b) and total stresses along the bridge (-c).

**Figure 12-b and -c** gives the vertical displacement and fibre stresses produced in the structure by a static load equal to 1250 kN applied on the top of the longitudinal stiff beam. It is worth mentioning that the stresses depicted in **Figure 12-c** consider both axial stresses and bending stresses. The results slightly overestimated the bridge deformability, with 32 mm of vertical displacement at the centre of the beam, compared with the 27 mm registered by LVDT-C7-FS/BS. A comparison between the experimental and numerical results in terms of total stresses is shown in **Figure 13**. The experimental results given in **Figure 13** were obtained from the average output obtained from each element and their symmetrical counterparts. The model accurately predicted the stress state of each element. The reliability of the model led to its being used for the further analyses described below.

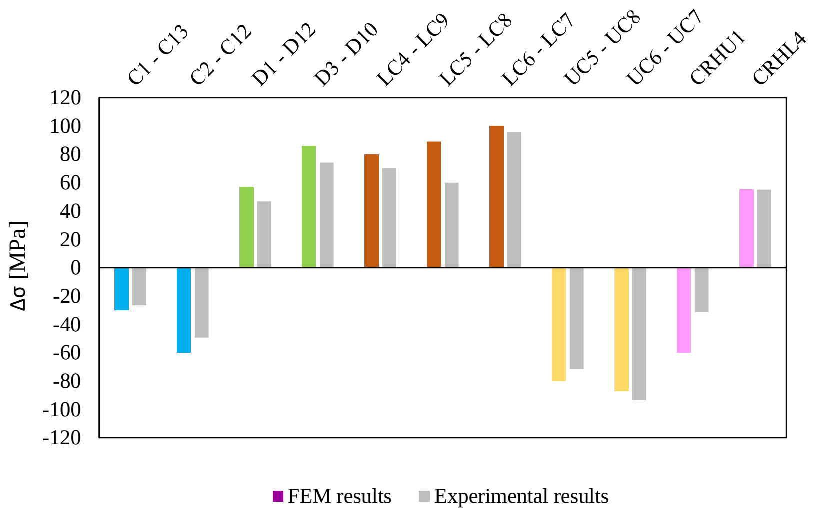


**Figure 13:** Comparison between experimental (grey bars) and FE results (coloured bars).

# 6. Analytical evaluation

## 6.1 Method

This method was defined for a general case and then applied specifically to the Quisi Bridge. The analytical assessment following this general method included: (i) load tests on the bridge, (ii) experimental results from the double experimental tests described in Sections 4 and 5, (iii) the numerical model validated by the full-scale test outputs, and (iv) the recommendations proposed by [10]. When all the experimental data is not available, this method also suggests the criteria to use.

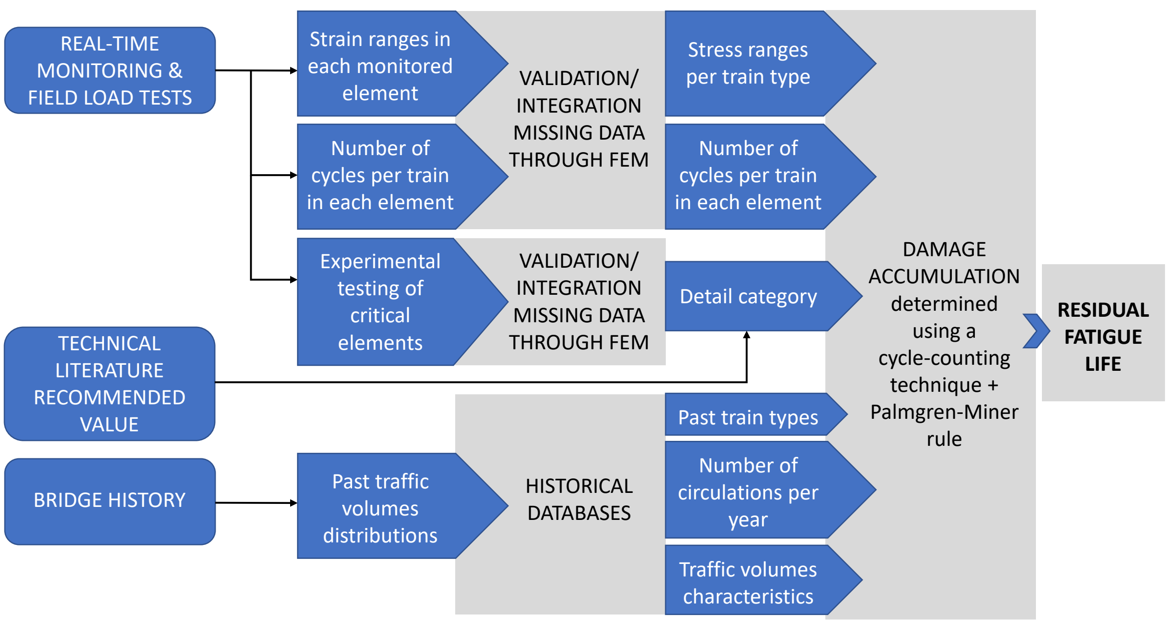


**Figure 14:** Relational flowchart of the proposed approach.

The method is organized into five steps summarized in the relational flowchart depicted in **Figure 14**:

1- Collection of information from past traffic volumes considering different train types (see Section 6.2).

2- Definition of (i) the number of cycles suffered by each element for each train type passing over the bridge and (ii) number of stress-increments in each type of element for a known type of train by real time monitoring during field load tests (see Section 6.2) if available or with the help of numerical simulations.

3- Extrapolation of stress ranges considering other types of trains and elements and validation throughout numerical simulations (see Sections 6.3 and 6.4).

4- Definition of detail category, depending on the available data:
   - Adoption of recommended values from [10][11][13], namely: detail category 71 and 100, depending on the expected triggered failure mechanism being normal or tangential, respectively.
   - Through fatigue failure tests of isolated elements such as the one described here and the application of damage accumulation rules such as the Palmgren-Miner rule recommended by EC3 (see Section 6.3).

5- Estimation of the remaining life of the bridge components applying damage accumulation rules, such as Palmgren-Miner (EC3) and the component's load history. For this, the current accumulated damage of each element is calculated for the subsequent projection of its remaining service life (see Section 6.4).

## 6.2 Load history and data from field load tests

Rolling loads on bridges such as those produced by vehicles cause variable amplitude stress distributions and typically a large number of cycles. In the broad field of fatigue assessment, the stress distribution can be determined using a cycle-counting technique such as the rainflow counting method. Current standards like the Eurocode 3 [10] for bridge fatigue assessment is based on the Palmgren-Miner rule to account for linear damage accumulation. Although structures with riveted joints are not explicitly referred to in EC3, several experimental investigations have classified these structures as detail category 71 [13]. In the present study, the damage accumulation rule was defined by coupling the stress distribution obtained from field load tests [29] together with the maximum stresses obtained in the elements of a 3D LSFE model of the whole bridge. The field tests on the Quisi Bridge were used to estimate its dynamic behaviour under the load of a specific train type (Train 9) [29].

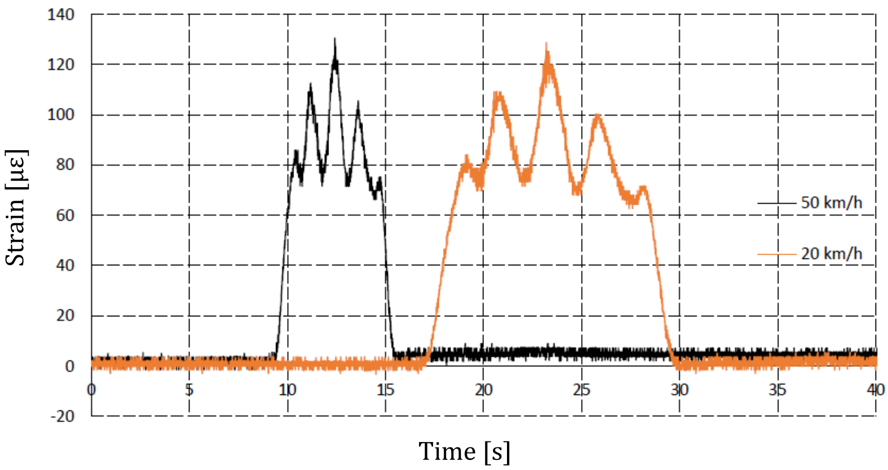


**Figure 15:** Strain distribution caused by the circulation of train 2500 in the central lower chord (isostatic span) assuming two different train velocities. Source: Ivorra et al. [29].

**Figure 15** gives the strain distribution monitored in the central lower chord of one of the isostatic spans. The measurements were taken at two different train speeds. **Figure 15** shows that the speed did not affect the maximum strain or the number of cycles obtained in the lower chord. The strain distribution of the most representative elements was compared to the numerical output obtained from a static analysis. The results of the field tests were used to evaluate: (i) cyclic stress characteristics associated with the different train loads. These results showed that cross-beams and stringers (longitudinal primary beams) are subjected to one cycle per axle, while all the other elements are subjected to lower cycles (cycles per train); (ii) the dynamic effect of train loads and the stress ranges in all the elements (the latter was deduced from the LSFE model). Deformation was found to increase by 30% in the field tests with respect to the FE analysis, resulting in a dynamic amplification factor of 1.3. The bridge's detail class was calculated from the information available on its loading history in service expressed by traffic volumes and their characteristics (see more details in Section 6.3). Assuming a period dating from 1915 to the present, 11 different types of train passed over the bridge, as can be seen in **Figure 16**.

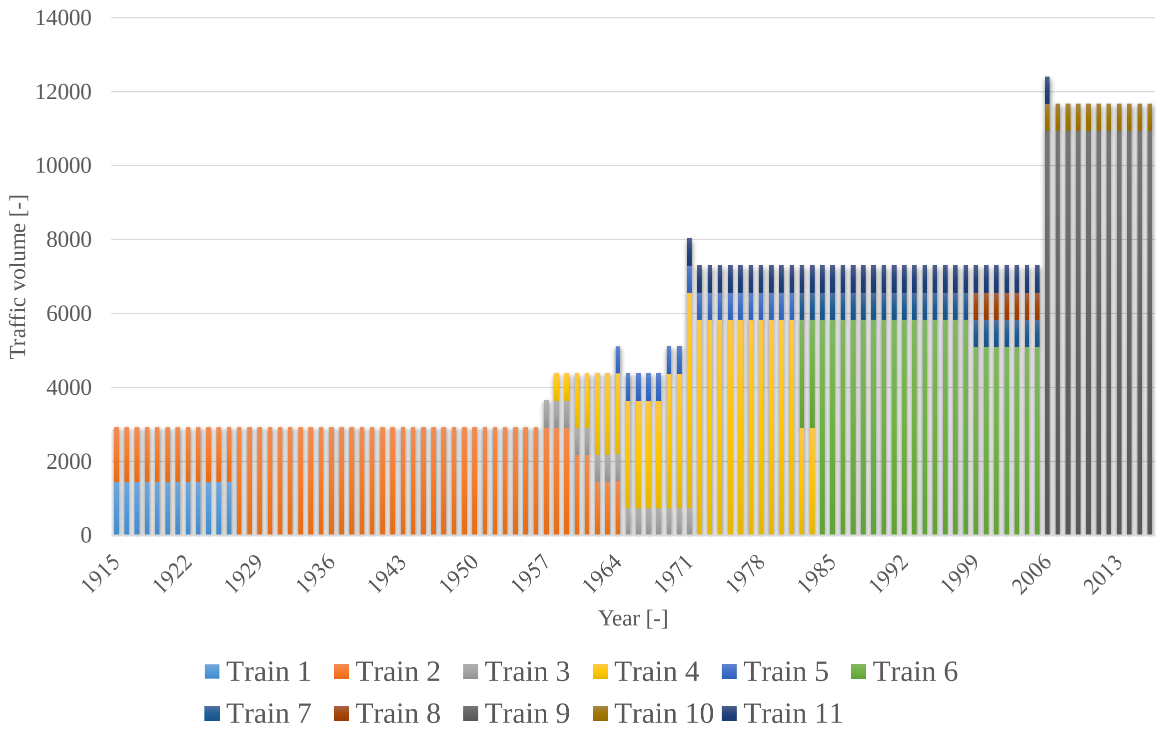


**Figure 16:** Loading history of the bridges during their exploitation expressed by train typology distributions over the years and traffic volumes. Data provided by the railway administration.

## 6.3 Definition of detail category based on test results

This section describes the calculation of the detail class of the cross beam from the experimental results described in Section 4, the information available on traffic volumes and the Eurocode 3 recommendations. The cross beam detail class was obtained assuming two different hypotheses: (i) trains were either completely loaded or (ii) only 80% loaded (this load is approximately the self-weight of the different train types). These two assumptions were made to take into account the uncertainty of the historical traffic loads. Past damage accumulation was deduced from the traffic volumes reported in **Figure 16** considering that the cross beam was 100% damaged during the lab test (i.e. after 31,377 cycles) and following the Palmgren-Miner rule. In detail, the total damage accumulation was divided into two parts: (i) damage accumulated during past train circulations and (ii) residual damage needed to reach the failure of the structure (100% damage as it was damaged during the lab test). In the first part, the accumulated damage was estimated as a function of the detail category (still unknown) and based on typical strain distribution patterns obtained in critical cross beams during field load tests. The information obtained during the real time field load tests allowed the calculation of the number of cycles per train passage and the strain increment associated with each circulation. In the second part, the number of cycles and the stress ranges applied to the element during the laboratory test were used to calculate the total damage of the cross beam as a function of the detail category. It is worth mentioning that the procedure adopted included a first hypothesis of the detail category which was then estimated by verifying that the complete damage (damage 100%) had been obtained after the laboratory test. In the 100% and 80% loading scenarios detail classes of 71 and 63 were deduced, respectively. The results, in terms of accumulated damage during consecutive periods of bridge operation from 1915 (blue bars) and the lab test (red bar) are given in **Figure 17-a and –b** and confirm that the cross beam would fail at detail category 71, for fully loaded trains, and at detail category 63 for 80% loaded trains.

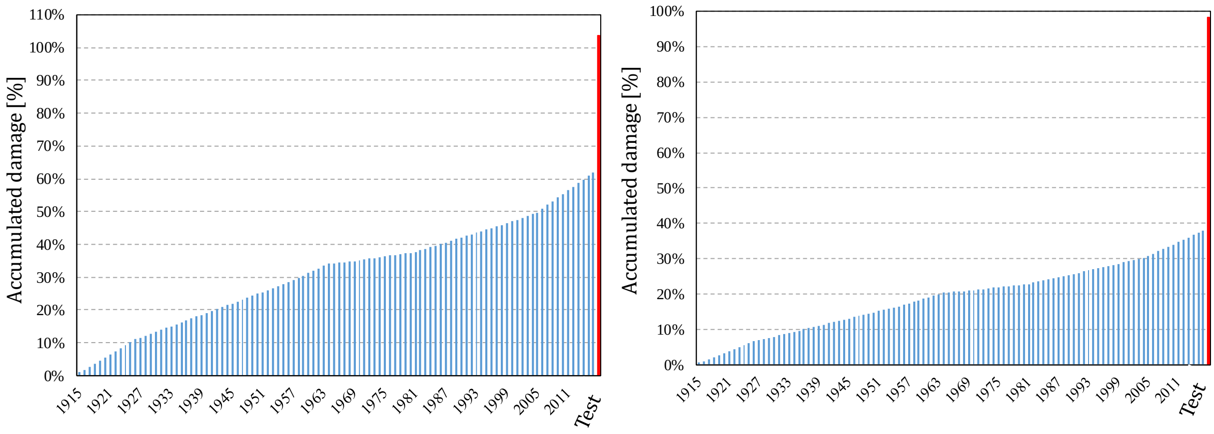


-a -b

**Figure 17:** Accumulated damage distributions over the bridges exploitation, considering: trains loaded at 100% (-a) and at 80% (-b).

## 6.4 Estimation of the remaining fatigue life

Remaining fatigue life can be analysed using LSFE models for stress amplitudes and the number of cycles undergone by each element. The Quisi Bridge was analysed adopting the LSFE model described above (see **Figure 18**). **Table 5** shows the results obtained for future traffic loads over the bridge (Train Type 9) without considering a dynamic amplification factor. In detail, strain increment patterns due to train circulation obtained from field load tests were used together with FE outputs to estimate the number of cycles per train circulation and the maximum stress ranges in the most critical elements composing the structure. This information was used to extrapolate the damage accumulated from 1915 till 2016.

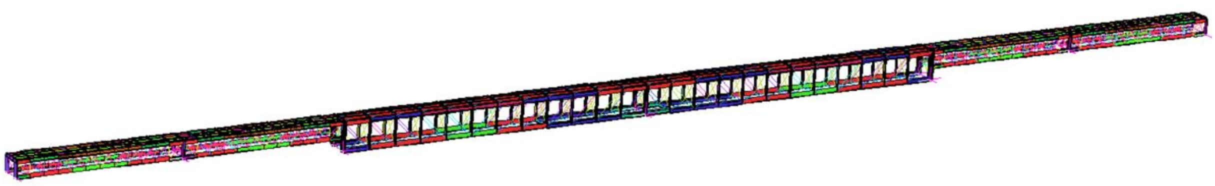

**Figure 18:** Finite Element model of the whole bridge, considering the strengthening and reparations introduced in the structure.

| **Table 5:** Maximum stress considering different structural elements. | | |
|---|---|---|
| **Structural Element** | | **Maximum stress [MPa]** |
| Lower chord | | 32.4 |
| Diagonal | | 29.7 |
| Cross beam | Axle 1 | 32.8 |
| | Axle 2 | 28.6 |
| Stringer | Axle 1 | 14.8 |
| | Axle 2 | 12.9 |

It is important to remember that, in this case, cross beams and stringers are directly subjected to the cycles produced by each axle, instead of 3 cycles per train, and therefore to higher accumulated damage than other elements. Considering a detail class equal to 71 or 63 for fully or 80% loaded trains, respectively (computation was performed in this case with detail class 63 but results are identical in both situations), assuming that the expected traffic volume in the next 10 years will consist of 32 type 9 trains per day and using the S-N curves method recommended by Eurocode 3, the damage caused in this period can be extrapolated.

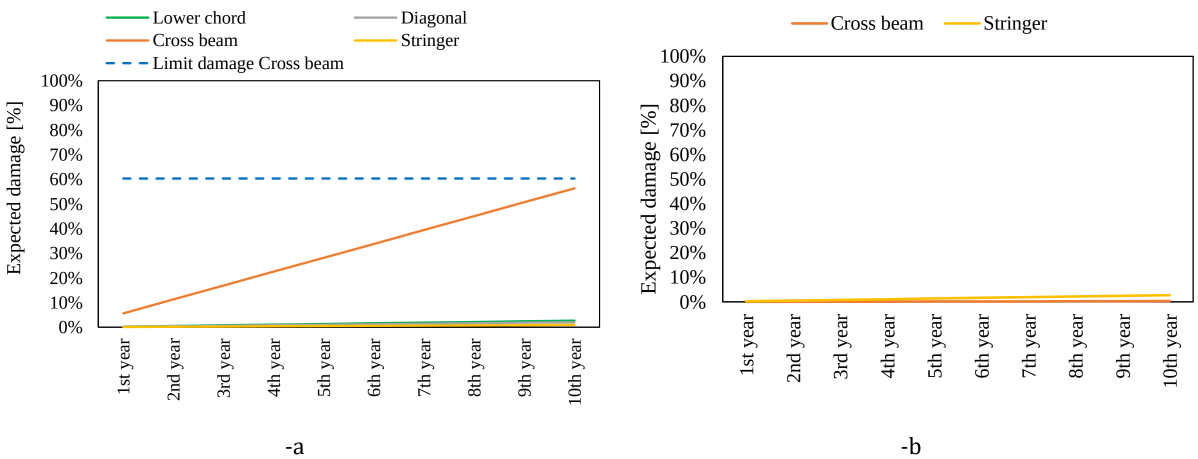


**Figure 19:** Expected accumulated damage in different structural elements considering: normal stresses (-a) and tangential stresses (-b).

**Figure 19-a** gives the damage percentages (due to normal stresses) expected to be accumulated in future train passages. This information must be coupled with the results illustrated in **Figure 17-b** which shows the percentages of past damage accumulated by the bridge during operational service using the detail category of 63 and 80% of the loaded trains. From that data it is possible to see that, before the laboratory test, the bridge accumulated (from 1915 to 2016) about 40% of damage. In the next 10 years, the cross beams will reach the 60% damage limit available considering a detail class 63 and 80% loaded train (Section 6.2), according to the information in **Figure 19-a**. The same calculation was repeated considering the tangential

stresses in the riveted connections taking into account the number of rivets composing the lateral connections of each element and the cross-section of each rivet. The results are given in **Figure 19-b** considering only cross beams and stringers and the lower detail class recommended by Eurocode 3 (80, the lowest in EC3). As can be seen in **Figure 19-b**, the damage expected in the next 10 years due to tangential stresses is quite low. Results from **Figure 19 -a and -b** confirm that the cross beams are the most vulnerable elements in the bridge (**Figure 19 -a**) and that normal stresses will be responsible for future fatigue damage (**Figure 19 -a and -b**).

## 7. Conclusions

This paper describes a study that aimed to provide meaningful experimental results on the fatigue behaviour of riveted steel railway bridges subjected to rolling loads in a combination of: (i) an ambitious experimental study with two full-scale tests to study local and overall bridge fatigue performance; and (ii) an analytical evaluation to assess the bridge's remaining fatigue life. The study was carried out on two riveted steel bridges in the Valencia railway network: the Quisi and Ferrandet Bridges, from which the following conclusions can be drawn:

- A cross beam element was subjected to a 0.55 Hz frequency cyclic load ranging from 50 to 650 kN to assess the local behaviour of the structure. The results showed that:
    - Fatigue cracks most probably nucleated after 10 k cycles and progressed fairly quickly until collapse at approximately 31k cycles.
    - The LVDT that monitored maximum vertical displacements was unable to capture any warning signs of imminent failure before 30k cycles, while strain gauges on the central section were able to track the redistribution of stresses as the cracks grew.
    - A fatigue test on a cross beam showed that fatigue cracks are likely to appear near to the central section. This finding could be explained by the peculiar geometry of the element and by the presence of an additional lower plate responsible for a sudden change in flexural stiffness.
    - Estimation of the detail class using the traditional S-N curves method found cross beam detail classes of between 63 and 71, depending on the uncertainties related to traffic loads.
- A full-scale fatigue test of an isostatic span was carried out to assess the structure's overall behaviour and reached the following conclusions:
    - The test identified the most heavily loaded elements and furnished the experimental results to calibrate a Finite Element model.

  - The fatigue test lasted for 45k cycles with a load range equal to 1250kN. During the lab investigation, the steel span showed elastic behaviour without the appearance of any fatigue damage. This confirmed that the non-primary elements of the bridge could be expected to operate safely for 27 more years.
- An analytical method based on load tests, numerical modelling, recommendations and codes was adopted to evaluate remaining bridge fatigue life. Its application to the bridge under study reached the following conclusion:
  - Fatigue calculations of the Quisi Bridge's remaining fatigue life identified the cross beams as the most vulnerable elements. Fatigue failures can be expected to arise in the next 10 years due to normal stresses, but not in the lateral riveted connections.

This work represents a step toward understanding the overall and local fatigue responses of old riveted steel bridges with a unique double experimental investigation. The results are expected to increase the existing fatigue test database: (i) confirmation of the detail category of steel riveted structures and (ii) the adoption of an analytical method applicable to other cases. A possible future extension of the present research line is represented by the evaluation of a wider number of critical principal elements (i.e. transversal girder and stringers) subjected to variable amplitude stress ranges, such as those produced in highway bridges.

## 8. Acknowledgements

The authors would like to express their gratitude to the FGV (*Ferrocarrils de la Generalitat Valenciana*) and *FCC Construcción S.A., CHM Obras e Infraestructuras S.A., Contratas y Ventas S.A.* and *CALSENS S.L.* for giving us the opportunity to test a bridge at the ICITECH facilities, also to Juan Antonio García Cerezo, of *FGV*, for his invaluable cooperation and recommendations. We also wish to show our gratitude for the magnificent work on the bridge by Eduardo Luengo, Salvador Ivorra, Juan J. Moragues, Benjamín Torres, Daniel Tasquer and Jesús Martínez. The tests on the bridge meant that much of the Structures Laboratory was out of service for other work, for which we owe a debt of gratitude to our *ICITECH* colleagues for their infinite patience and understanding.

## 9. References

[1] M. Kużawa, T. Kamiński, J. Bień, Fatigue assessment procedure for old riveted road bridges, Archives of Civil and Mechanical Engineering, v 18- 4, 2018, pp 1259-1274.

[2] B. Pedrosa, J. A. F. O. Correia, C. Rebelo, G. Lesiuk, M. Veljkovic, Fatigue resistance curves for single and double shear riveted joints from old portuguese metallic bridges, Engineering Failure Analysis,v 96, 2019, pp 255-273.

[3] L. Sieber, R. Urbanek, J. Bär, Crack-Detection in old riveted steel bridge structures, Procedia Structural Integrity,v 17, 2019, pp 339-346.

[4] A.M.P. De Jesus, A.L.L. da Silva, M.V. Figueiredo, J.A.F.O. Correia, A.S. Ribeiro, A.A. Fernandes, Strain-life and crack propagation fatigue data from several Portuguese old metallic riveted bridges, Eng. Fail. Anal., v 18-1, 2011, pp. 148-163.

[5] D. Leonetti, J.Maljaars, G. Pasquarelli, G. Brando, Rivet clamping force of as-built hot-riveted connections in steel bridges, Journal of Constructional Steel, v 167, 2020;

[6] D. Leonetti, J.Maljaars, H. H. Snijder, Fatigue life prediction of hot-riveted shear connections using system reliability, Engineering Structures,v 1861, 2019, pp 471-483.

[7] H. Heydarinouri, A. Nussbaumer, J. Maljaars, E. Ghafoori, Proposed criterion for fatigue strengthening of riveted bridge girders, Procedia Structural Integrity,v 19, 2019, pp 482-493.

[8] Z. Liu, M. Hebdon, J. Correia, H. Carvalho, P. Vilela, A. De Jesus, R. Calçada, Fatigue assessment of critical connections in a historic Eyebar suspension bridge, J. Perform. Constr. Facil., v 33-1, 2019.

[9] A. Taras, R. Greiner, Development and application of a fatigue class catalogue for riveted bridge components, Struct. Eng. Int., v 20-1, 2010, pp. 91-103.

[10] CEN, EN 1993-1-9: Eurocode 3, Design of Steel Structures – Part 1–9: Fatigue, European Committee for Standardization, Brussels (2005).

[11] American Association of State Highway and Transportation Officials (AASHTO), Guide Specifications for Fatigue Evaluation of Existing Steel Bridges, Washington, D.C., (1990).

[12] American Railway Engineering and Maintenance of way Association (AREMA), Manual for Railway Engineering, (2019).

[13] B. Kühn, M. Lukic, A.Nussbaumer, H.P.Günther, R. Helmerich, S.Herion, M.H.Kolstein, S. Walbridge, B.Androic, O. Dijkstra, and Ö. Bucak, Assessment of existing steel structures: Recommendations for estimation of the remaining fatigue life. EUR - Scientific and Technical Research Series, Luxembourg, 2008.

[14] A. Cunha, E. Caetano, F. Magalhães, C. Moutinho, Recent perspectives in dynamic testing and monitoring of bridges, J Struct Control Health Monit, v 20-6, 2012, pp 853-877.

[15] F. Magalhães, A. Cunha, E. Caetano, Vibration based structural health monitoring of an arch bridge: from automated OMA to damage detection, MechSyst Signal Process, v 28, 2012, pp 212-228.

[16] J. Leander, A. Andersson, R. Karoumi, Monitoring and enhanced fatigue evaluation of a steel railway bridge, EngStruct, v 32, 2010, pp 854-863.

[17] B. Caglayan, K. Ozakgul, O. Tezer, Fatigue life evaluation of a through-girder steel railway bridge, Eng Failure Anal, v 16-3, 2009.

[18] B. M. Imam, T. D. Righiniotis, M. K. Chryssanthopoulos, Numerical modelling of riveted railway bridge connections for fatigue evaluation, Engineering Structures, v 29-11, 2007, pp 3071-3081.

[19] A.H. DePiero, R.K. Paasch, S.C. Lovejoy, Finite-element modelling of bridge deck connection details, J Bridge Eng (ASCE), v 7-4, 2002, pp 229-235.

[20] M. Al-Emrani, R. Kliger, FE analysis of stringer-to-floor-beam connections in riveted railway bridges, J Constr Steel Res, v 59-7, 2003, pp 803-818.

[21] M. Al-Emrani, Fatigue performance of stringer-to-floor-beam connections in riveted railway bridges, J Bridge Eng (ASCE), v 10-2, 2005, pp 179-185.

[22] J. Tulonen, T.Siitonen, A. Laaksonen, Behaviour of riveted stringer-to-floorbeam connections in cyclic load tests to failure, Journal of Constructional Steel Research, v 160, 2019, pp 101-109.

[23] A. Pipinato, M. Molinari, C. Pellegrino, O. S. Bursi, C. Modena, Fatigue tests on riveted steel elements taken from a railway bridge, Struct. Infrastruct. Eng., v 7-12, 2009, pp 907-920.

[24] A. Pipinato, C. Pellegrino, O. S. Bursi, C. Modena, High-cycle fatigue behavior of riveted connections for railway metal bridges, J. Constr. Steel Res., v 65, 2009, pp 2167-2175.

[25] A. De Jesus, M. Figueiredo, A. Ribeiro, P. Castro, A. Fernandes, Residual lifetime assessment of an ancient riveted steel road bridge, Strain, v 47-1, 2011, pp 402-415.

[26] A. Azizinamini, "Full scale testing of old steel truss bridge." Journal of Constructional Steel Research, v. 58-5–8, 2002, pp 843–858.

[27] UNE EN ISO 6892-1:2017: Metallic materials - Tensile testing - Part 1: Method of test at room temperature (ISO 6892-1:2016).

[28] UNE EN ISO 148-1:2017: Metallic materials - Charpy pendulum impact test - Part 1: Test method (ISO 148-1:2016).

[29] S. Ivorra, M. Buitrago, E. Bertolesi, B. Torres, and D. Bru, Dynamic identification on an ancient steel bridge of six spans, 14th International Workshop on Advanced Smart

Materials and Smart Structures Technology (ANCRiSST), V. Gattulli, O. Bursi, and D. Zonta, eds., Sapienza. UniversitàEditrice, Rome, 139–142, 2019.